had a rate coefficient of 7×10^{-11} and 4.5×10^{-13} cm^3 molecule^{-1} s^{-1} assuming reaction 13 to be negligibly slow. As we have already pointed out, whether or not reaction 13 proceeds facilely is subject to some controversy. Even Quiñones et al.'s[21] value for this rate coefficient, however, is substantially lower than the upper limit used in Cheah and Clyne's model calculations, so would probably tend to support their smaller value for k_2. Given that Cheah and Clyne's calibration of their resonance lamp used to determine $N(^2D)$ number densities was indirect, their estimated value for k_2 of $(4-6) \times 10^{-13}$ cm^3 molecule^{-1} s^{-1} also agrees adequately with our findings. Our measurement is a direct determination and should be preferred.

Throughout these studies [NF(a)] was always independent of $[H_2]$ added. No decrease in [NF(a)] could be seen even though sensitivity was more than adequate to see a 10% degradation. These observations establish an upper limit for H_2 quenching of NF(a) of 1×10^{-14} cm^3 molecule^{-1} s^{-1}. This can be compared to an earlier measurement of D_2 quenching of NF(a) by Kwok et al.[23] who reported a value of $k < 7 \times 10^{-14}$ cm^3 molecules^{-1} s^{-1}, and the recent measurements of Quiñones et al.,[21] who obtained $k = 6.4 \times 10^{-16}$ and 3.2×10^{-16} cm^3 molecule^{-1} s^{-1} for NF(a) quenching by H_2 and D_2, respectively.

Using vacuum-UV resonance fluorescence to monitor $N(^2D)$ and $N(^4S)$,[11] we have observed initial formation only of $N(^2D)$, with $N(^4S)$ appearing only later in the reaction, presumably as a result of $N(^2D)$ quenching. Cheah and Clyne[2,3] made similar observations and suggested that the primary product channel was to make $N(^2D)$. Absolute photometric measurements we have made of NF(a), $N(^2D)$, and $N_2(B)$ temporal profiles resulting from reactions 1 through 3, and which we shall report soon,[11] are fully consistent with a branching ratio for $N(^2D)$ formation in reaction 2 of unity. This is the result predicted by spin and orbital angular momentum correlation rules.[22]

Given that $N(^2D)$ is a key precursor for $N_2(A)$ formation via reaction 3, reaction 2 presents a kinetic bottleneck for this $N_2(A)$ generation scheme. Due to its relatively small rate coefficient, large H and NF(a) concentrations will be required in a generator to produce enough $N(^2D)$ to drive reaction 3. This is further exacerbated by the reactivity of $N(^2D)$ with generator surfaces and with other generation species such as NF_2, NF, H_2, and HF. However, the small value of k_2 at room temperature suggests the presence of an energy barrier, such that either elevated temperature or modest vibrational excitation of the NF(a) might provide a means for accelerating the reaction rate substantially.

Acknowledgment. We appreciate financial support from the Air Force Weapons Laboratory under Contract F-29601-84-C-0076. Insightful comments from our PSI colleagues, Dave Green, Bill Marinelli, and George Caledonia, benefited our efforts. Henry Murphy and Warren Savage's experimental assistance proved invaluable.

Registry No. H, 12385-13-6; NF, 13967-06-1.

Laser-Induced Fluorescence Spectroscopy of the $B^2\Pi$, $A^2\Delta$, and $C^2\Sigma^+$ States of the NS Radical

Jay B. Jeffries,* David R. Crosley, and Gregory P. Smith

Chemical Physics Laboratory, SRI International, Menlo Park, California 94025 *(Received: December 7, 1987)*

Laser-induced fluorescence has been used to study the $B^2\Pi$, $A^2\Delta$, and $C^2\Sigma^+$ excited states of the NS free radical in a low-pressure discharge flow system. Excitation scans were recorded exciting $v' = 0$–12 in B, $v' = 0$ and 1 in A, and $v' = 0$ in C. Numerous perturbations appear in excitation scans to the B state through anomalous Λ-doublet splittings and line intensities. Fluorescence spectra have been recorded through $v'' = 26$ in $X^2\Pi$ and have been used to determine vibrational term values in the ground state. Vibrational band transition probabilities have been measured for 236 bands in the B–X system, 10 bands in A–X, and 5 in C–X. The electronic transition moment for the B–X system is constant with internuclear distance, while that for C–X decreases with increasing distance.

Introduction

The NS radical possesses a large number of excited electronic states in the energy region 30 000–45 000 cm^{-1} above the ground $X^2\Pi$ state. These include both valence and Rydberg doublet states, as well as quartet states whose presence and spectroscopic constants have been inferred from perturbations of the doublets. This overall state structure has features in common with the more familiar, isovalent NO molecule, although in NS the valence states lie significantly lower in energy.

These states in NS are readily accessible to detection by laser-induced fluorescence (LIF) using tunable lasers together with standard nonlinear frequency conversion techniques. The NS radical is thereby amenable to two types of useful studies. The first type is collisional energy transfer, both internal (v,J,Ω) transfer within an electronic state, and state-specific quenching (total removal) and electronic-to-electronic transfer. For example, we have used the time dependence of LIF signals to investigate vibrational-level-specific total decay rates of the $B^2\Pi$ state.[1] The v' dependence of the decay rate varied with collision partner in both direction (increasing or decreasing) and magnitude, indicating interesting dynamic effects tied to the structure of the collider. In similar experiments on higher lying vibrational levels of $B^2\Pi$, the effects of perturbations on the collision-free decay and on collisional removal by N_2 were studied.[2] The many nearby electronically excited states in NS, having different electronic structure, and each accessible by laser excitation and fluorescence studies, make this radical a fertile ground for such collision studies.

The other type of study is the detection of NS in practical systems where it may play a chemical role. An example of this is the important area of combustion chemistry.[3] The radical had not previously been considered in this context, but we recently detected it in simulated coal flames,[4] that is, methane burning in oxygen with minor amounts (a few percent) of added NH_3 and H_2S. The detection was by LIF in the C–X system, and the absolute radical concentrations were deduced by using spectro-

(1) Jeffries, J. B.; Crosley, D. R. *J. Chem. Phys.* **1987**, *86*, 6839.

(2) Matsumi, Y.; Munakata, T.; Kasuya, T. *J. Phys. Chem.* **1984**, *88*, 264.

(3) Kaufman, F. *Proceedings of the Nineteenth Symposium (International) on Combustion*; The Combustion Institute: Pittsburgh, PA, 1982; p 1.

(4) Jeffries, J. B.; Crosley, D. R. *Combust. Flame* **1986**, *64*, 55.

0022-3654/89/2093-1082$01.50/0

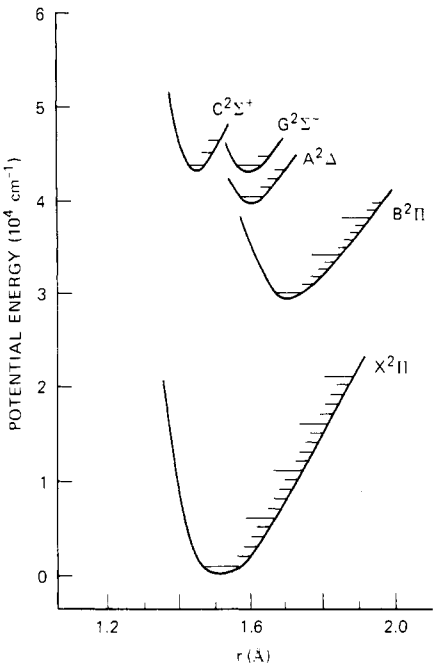

Figure 1. Potential energy curves and vibrational levels for the states of NS studied here.

scopic parameters from a variety of sources (including the present work) and quenching rates estimated by analogy to studies of similar molecules. Uncertainties in the final absolute concentrations were estimated to be a factor of 3, which was sufficiently accurate to demonstrate that a large fraction of the fuel sulfur and fuel nitrogen was processed through the NS radical. (Relative concentration changes, for example, when varying the S to N ratio, had a much higher precision.) This raises interesting and important questions concerning a major unsolved combustion problem, the interaction between the formation of NO_x and SO_x in flames.[5] Too little is known about the reactions of NS to ascertain its direct importance as a reaction intermediate, but the ease of LIF detection of NS suggests that it could be used to follow the course of the N–S interactive chemistry.

Both types of study require well-determined spectroscopic parameters for the band systems involved. A study of the LIF spectroscopy of several of these states is the topic of the present study. Potential energy curves for those states, $B^2\Pi$, $A^2\Delta$, $G^2\Sigma^-$, and $C^2\Sigma^+$, together with $X^2\Pi$, are shown in Figure 1. In most cases, the structural constants (Dunham coefficients) are known well from previous measurements on chemiluminescent emission spectra, produced when H_2S, SCl_2, or S_2Cl_2 is added to a low-pressure nitrogen discharge. This includes a comprehensive study of many states (including all those studied here) by Jenouvrier and co-workers[6-8] and earlier work on the $B^2\Pi$ state by Narasimham and Subramanian.[9,10] Our measurements began by using that information to provide facile identification of the LIF spectra. On the other hand, the lack of spectral congestion following state-specific laser excitation,[11] even in low-resolution fluorescence scans, has enabled us to identify many new bands with high-lying v'', and thus provide improved values of ω_e and $\omega_e x_e$ for $X^2\Pi$. Much of our focus has been on intensity measurements, i.e., band emission strengths and radiative lifetimes, for the B–X, A–X, and C–X systems; vibrational transition probabilities are reported for a large number of bands belonging to the three systems. We have also observed the $G^2\Sigma^-$ state via LIF and report some interesting collisional behavior near the predissociation limit for B and A.

Experimental Method

NS was produced in its ground electronic state via gas-phase chemistry occurring in a low-pressure discharge flow reactor. For most of the measurements reported here, a mixture containing 300 mTorr of N_2 and 10 mTorr of SF_6 in a He carrier at about 1 Torr total pressure flowed through a microwave discharge. (In a few measurements, SCl_2 vapor was entrained in He and added downstream of a discharge in an He flow containing a partial pressure of ~30 mTorr of N_2.) For the spectroscopic measurements, the flow rates and pressures were generally adjusted to produce optimum signal. For cases where collisions are or could be important, more care was taken concerning the ambient environment, as described in ref 1.

The NS molecules were excited by using light from a frequency-doubled dye laser with a pulse length of 10 ns and bandwidth (in the ultraviolet) of ~0.3 cm^{-1}. Operation at the many different wavelengths required was accomplished primarily through frequency conversion by stimulated Raman shifting in H_2. A judicious choice of Stokes and anti-Stokes shifts permitted all the measurements reported here to be carried out with only three dyes. The fluorescence was focused at right angles onto the entrance slit of a 0.35-m monochromator and detected with a photomultiplier tube. An EMI 9558Q was used for most measurements, although an RCA 31034 was needed for some of the B–X bands far in the red. The amplified photomultiplier signal was fed to a boxcar integrator for gated or pulse-integrated measurements, or into an oscilloscope or a transient digitizer for time-resolved decays. The laser radiation which passed through the flow reactor cell was monitored by a photodiode whose output fed into a second boxcar channel, and used for normalization to laser power.

Initial NS signals were observed in copious amounts in the N_2/SF_6 mixture, and no attempt was made to use a more sophisticated production method until the commencement of the collision measurements. However, large concentrations of S_2 molecules were also produced in this system. LIF in the $B^3\Sigma_u^- - X^3\Sigma_g^-$ system[12] of S_2 was readily observed in the vicinity of the B–X system of NS, and in many cases the absorption bands of the two molecules overlapped one another. When this gave rise to interferences, the S_2 and NS spectra were separated by time resolution using the boxcar gate. The radiative lifetime of $B^2\Pi$ NS is ~1 μs (see below), much longer than that of $B^3\Sigma_u^-$ S_2, which is 36 ns.[13] Therefore, using a gate with a 150-ns width but a leading edge some 150 ns after the laser pulse discriminated strongly against LIF from S_2, while detecting most of the NS LIF.

The response of each monochromator/photomultiplier combination was calibrated by using standard tungsten and deuterium lamps.[14] A cutoff filter, with separately measured transmission, was used to block second-order ultraviolet transitions when observing bands in the red. The monochromator wavelength calibration was checked by using a series of Hg emission lines in the ultraviolet and visible regions. The laser wavelength dial was roughly calibrated by using LIF of OH present in a glassblower's torch flame, but precise analysis of the excitation spectra was not attempted because the laser bandwidth was not narrow enough to give spectroscopic information superior in accuracy to that determined previously in the emission studies.[6-10]

Excitation Scan Results

Figures 2–6 exhibit excitation scans for each of the electronic states studied. Scans were taken pumping $v' = 0$–12 in $B^2\Pi$, $v' = 0$ and 1 in $A^2\Delta$, and $v' = 0$ in $C^2\Sigma^+$ and $G^2\Sigma^-$. In each case, the monochromator was set to detect a bright fluorescence band, although it was not always the most intense one for that v'.

(5) Levy, A. *Proceedings of the Nineteenth Symposium (International) on Combustion*; The Combustion Institute; Pittsburgh, PA, 1982; p 1223.
(6) Jenouvrier, A.; Pascat, B. *Can. J. Phys.* **1973**, *51*, 2143.
(7) Vervloet, M.; Jenouvrier, A. *Can. J. Phys.* **1976**, *54*, 1909.
(8) Jenouvrier, A.; Pascat, B. *Can. J. Phys.* **1980**, *58*, 1275.
(9) Narasimham, N. A.; Subramanian, T. K. B. *J. Mol. Spectrosc.* **1969**, *29*, 294.
(10) Narasimham, N. A.; Bala Subramanian, T. K. *J. Mol. Spectrosc.* **1971**, *40*, 511.
(11) Crosley, D. R. *J. Chem. Educ.* **1982**, *59*, 446.
(12) Anderson, W. R.; Crosley, D. R.; Allen, Jr., J. E. *J. Chem. Phys.* **1979**, *71*, 821.
(13) Quick, Jr., C. R., Weston, Jr., R. E. *J. Chem. Phys.* **1981**, *74*, 4951.
(14) Optronics Laboratories, Orlando, FL.

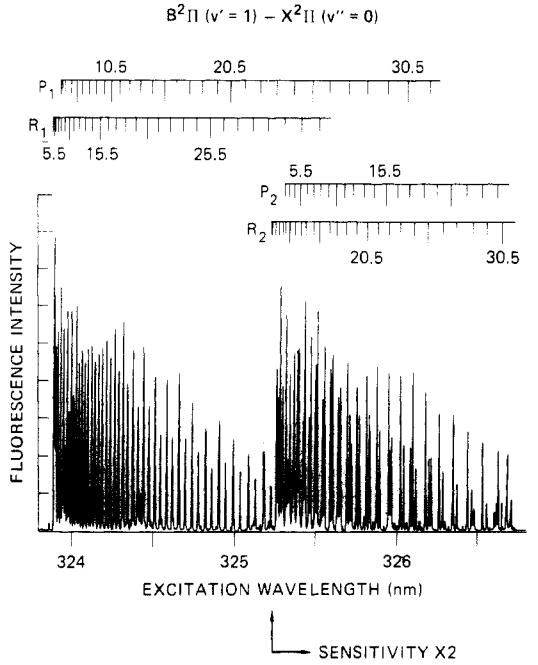

Figure 2. Excitation scan for the (1, 0) band of the B–X system, showing individual rotational lines for each of the spin–orbit subbands. The F_1 level is that with $\Omega = {}^1/_2$ and the F_2 level has $\Omega = {}^3/_2$.

A. B–X Excitation Scans. An excitation scan for the (1, 0) band of the B–X system is shown in Figure 2. The appearance is typical for all of the unperturbed bands of this parallel transition, showing R-branch heads, P branches shaded to the red, and no Q branches. Because both states are strongly in the Hund's case a limit, the $\Delta\Omega \neq 0$ subbands should be weak. In two vibrational bands, a search was made for the $\Omega = 3/2 \leftarrow 1/2$ subband, which should be in a spectrally clean region 90 cm^{-1} to the blue of the $1/2 \leftarrow 1/2$ subband. Upper limits of 0.03 and 0.10 are placed on the ratio of intensities of the $3/2 \leftarrow 1/2$ to the $1/2 \leftarrow 1/2$ subbands, respectively, for the (1,0) and (9,0) vibrational bands. The relative intensities of the two main subbands ($\Delta\Omega = 0$) are governed primarily by the thermal population difference of the spin–orbit components in the ground state.

For a quantitative comparison of the excitation scans with earlier emission spectra,[7,9,10] the line positions of all four branches of the unperturbed (9, 0) band were computed using the constants given in ref 7. The average deviation between measured and calculated relative line positions in the 1/2–1/2 and 3/2–3/2 subbands were, respectively, 0.03 and 0.07 cm^{-1}; recall that the laser bandwidth is ~0.3 cm^{-1}. (From this comparison the absolute laser frequencies differed from the nominal setting by +0.54 and +0.47 cm^{-1} for the two subbands, well within the dial calibration.) Each absorption line consists of a closely spaced doublet, due to the Λ-doubling in each Π-state. This is typically observed in the spectra as a broadening of the rotational lines with increasing J. For example, in the (0, 0) band the observed line width is determined by the laser bandwidth at low J, but the lines broaden smoothly to 1.1 cm^{-1} at $N = 26$. Our spectra are not of high enough resolution to provide spectral constants improved over those determined in ref 6–10, and we have not attempted a rotational analysis.

An analysis of the excitation scans to yield vibrational term values has, however, been made. The bandhead positions are measured, and the band origins were determined from these by using the previous rotational analyses.[6,8] The results are $\omega_e = 794.9 \pm 0.9$ cm^{-1} and $\omega_e x_e = 3.72 \pm 0.12$. This compares favorably with the standard values[7,9,10] of 798.0 and 3.65 cm^{-1}.

B. Perturbations in $B^2\Pi$. Perturbations are evident throughout the B–X emission spectra. These show up as displacements of lines from their anticipated, calculated position, large amounts of Λ-doublet splitting, and anomalous intensities. In fact, in these uncongested excitation spectra, unusual Λ-doublet splitting and line intensities constitute better indicators of perturbations than

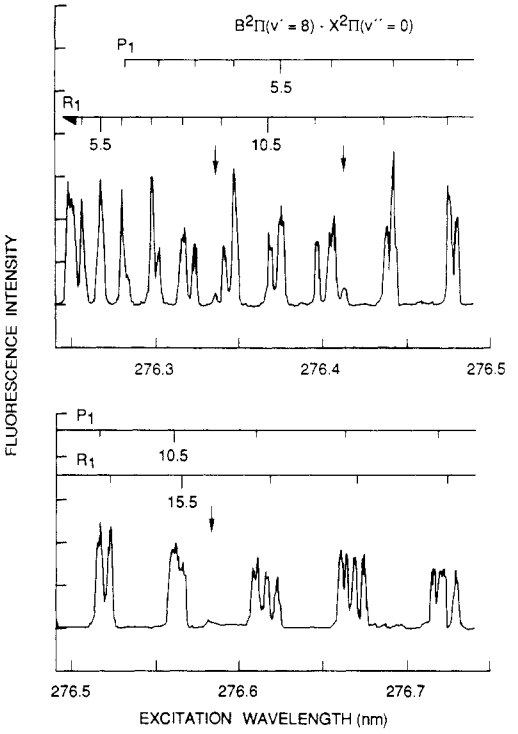

Figure 3. Excitation scan for the (8,0) band of the B–X system; $v' = 8$ is known to be perturbed by the nearby $B'^2\Sigma^+$ state. Note the large Λ-doublet splitting for the R_1 branch, $J'' = 16.5$–19.5. The arrows show the positions of $B'^2\Sigma^+$ lines as expected from the analysis presented in ref 8.

do line displacements; they appear even when the central line shift is less than the laser bandwidth. Figure 3 shows two contiguous regions of the (8, 0) band and illustrates a series of perturbed levels in $v' = 8$. Note in the upper panel the width of the relatively unperturbed lines, each of which is a doublet. In the lower panel appear several lines with much larger splittings. Also present in this spectrum are a number of weaker lines, indicated by the arrows. These[6] are excitation to the perturbing $B'^2\Sigma^+$, $v' = 0$, level, which interacts with the entire $v' = 8$ level of $B^2\Pi$. (Fluorescence decay curves reported in ref 2 show double-exponential traces for several J in $v' = 8$, further evidence of the state mixing in this vibrational level.)

Perturbations are seen in other vibrational levels as well. We have identified all of the perturbations with $J < 30.5$ which are listed in ref 8, where they were used to deduce information on the spectroscopic constants of the perturbing states, $B'^2\Sigma^+$, $b^4\Sigma^-$, and $a^4\Pi$. Known[8] perturbed lines with higher J are too weak in our excitation scans. In addition, we see perturbations not catalogued in ref 8. For example, intensity perturbations are evident in the F_2 component ($\Omega = {}^3/_2$) of $v' = 0$, $J' = 17.5$–20.5. In $v' = 1$, there is a previously[8] seen perturbation near $F_2(10.5)$, and newly observed ones near $F_2(18.5)$, although the displayed spectrum in Figure 2 is too compressed to exhibit them clearly. In $v' = 4$ and 5, the entire F_1 component shows anomalously large Λ-doublet splitting; in $v' = 3$ and 6, the F_2 component shows large doubling (though less than for F_1 in 4 and 5). Λ-doubling is large in $v' = 8$ and smaller, but still large and resolvable, in $v' = 9$ and 10.

Figure 4 shows the high-J portion of an excitation scan of the (12, 0) band of the B–X system. This is the highest bound level of the $B^2\Pi$ state and is strongly affected by perturbations and predissociation. There are many lines (not shown here) with anomalously large Λ-doublet splitting, particularly in the ${}^1/_2$–${}^1/_2$ subband; there are also displaced lines, for example, $P_1(23.5)$ seen here. At lower J values in the F_1 component, lines from $B^2\Sigma^+$ can be seen as well. There are no lines beyond those seen in Figure 4, which belong to the levels $F_1(25.5)$ and $F_2(17.5)$ in $B^2\Pi$. This breaking off of the fluorescence spectrum is due to the onset of predissociation for higher lying levels, confirming the dissociation

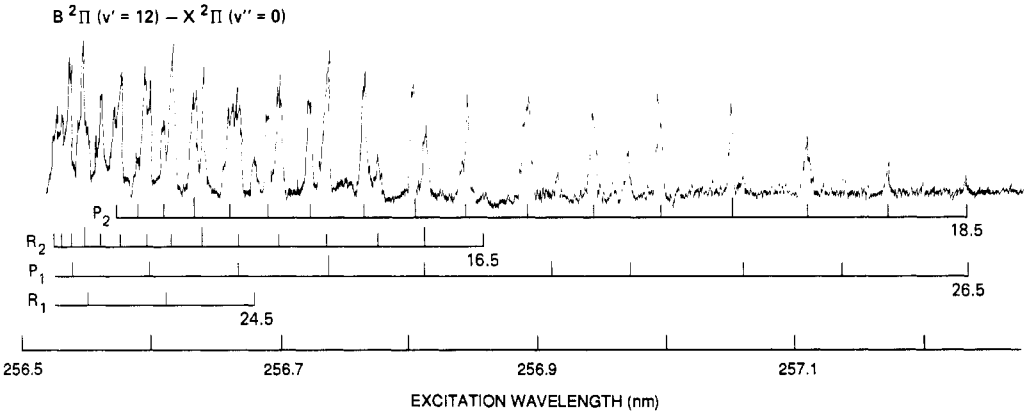

Figure 4. Excitation scan for the high-J portion of the B–X (12,0) band, showing the cessation of fluorescence above $F_2(17.5)$ and $F_1(25.5)$, due to the onset of predissociation.

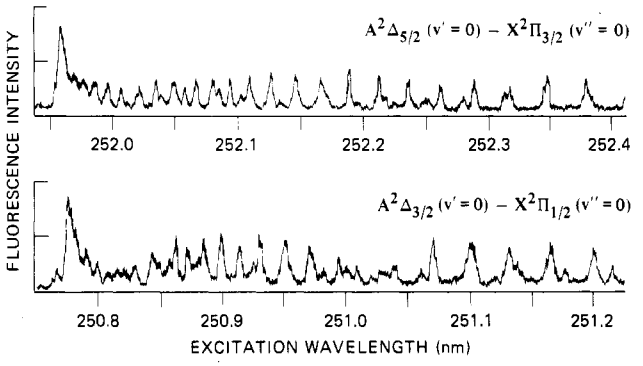

Figure 5. Excitation scans for the two spin–orbit subbands of the (0,0) band of the A–X system. The bandheads at shortest wavelengths are formed by R branches; Q and P branches are also present in this perpendicular transition. This band has not been rotationally assigned but the analysis is available from ref 6.

limit determined in ref 6 by the cessation of emission at the corresponding positions. The overall intensity of the (12, 0) band is weak, due at least in part to its short lifetime (see below) and the correspondingly reduced quantum yield.

In many of the B–X bands there exists a single weak line between 1 and 6 cm^{-1} to the blue of the R_1 head (see Figure 2). This line is about 3 cm^{-1} blue of the calculated $Q(^1/_2)$ which is too large for the Λ-doubling of this line. The line does not correspond to another isotope, and we have been unable to determine its origin. We also can see bandheads due to the $N^{34}S$ isotope (natural abundance 4%) in the calculated positions.

C. Excitation Scans for Other States. The $v' = 0$ and 1 levels of the $A^2\Delta$ state have been excited; Figure 5 shows excitation scans of the two spin–orbit subbands of the (0, 0) band of the A–X system. This is a perpendicular transition containing P, Q, and R branches. The A–X excitation spectra have not been assigned but the analysis given in ref 7 is available for that purpose. Although not shown in the figure, the region encompassing the $^2\Delta_{3/2}$–$^2\Pi_{3/2}$ subband was scanned but no LIF was seen; it thus has an intensity <20% of the main subbands.

The top portion of Figure 6 shows an excitation scan of the (0, 0) band of the C–X system. This is the characteristic four-headed pattern of a $^2\Sigma$–$^2\Pi$ transition, showing here P and Q heads for this transition shaded to the violet. As with the A–X transition, we have not performed a detailed rotational analysis or assignment, although the lines are readily identifiable by using the results presented in ref 6. It was this transition which was used for the detection of NS in flames;[4] in the hot flame environment many more high-lying rotational levels are populated and could be excited by the laser. Identification of certain specific transitions was of course necessary for those quantitative measurements of NS concentrations.

Slightly to the red of the (0, 0) band of the C–X system lies the (0, 0) band of the $G^2\Sigma^-$–$X^2\Pi$ system. An excitation scan of the two branches of this red-degraded system is shown in the

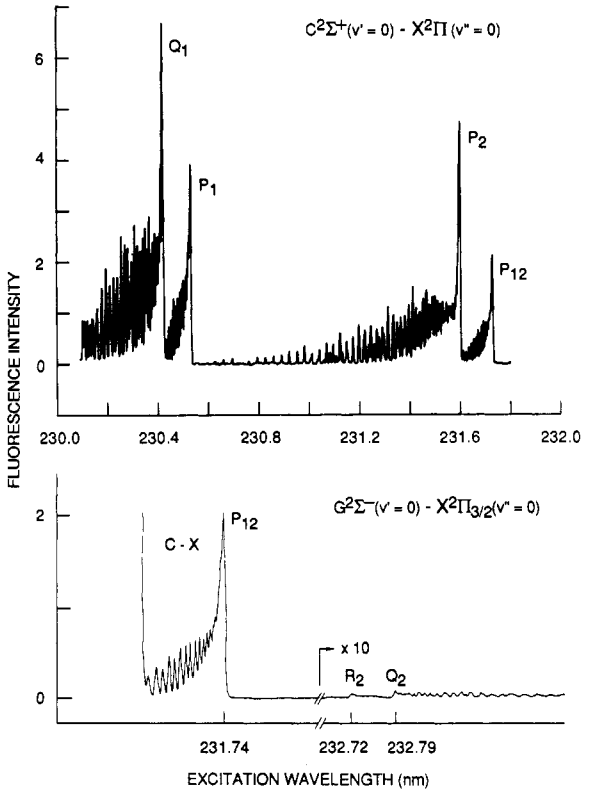

Figure 6. (Top) Exciation scan for the (0,0) band of the C–X system. Bandheads are marked although a full rotational analysis has not been performed. (Bottom) Excitation scan for the F_2 region of the G–X transition (0,0) band, together with the P_{12} bandhead of C–X(0,0) for comparison. Note the tenfold increase in sensitivity for G–X.

bottom part of Figure 6. The intensity of this band in our experiment is much lower than that of the (0, 0) band of the C–X system. This contrasts with the qualitative observation of intense emission upon its first discovery, as quoted in ref 6. According to Franck–Condon factor calculations (see below), we are pumping and observing relatively bright bands, about as strong as those in C–X. Hence we do not understand the reason for the low LIF intensity compared with that in the emission spectra. However, we abandoned further LIF measurements on G–X within the current study.

A brief search was made for the (0, 0) band of the $H^2\Pi$–$X^2\Pi$ system, which should lie near 228 nm, at slightly shorter wavelengths than for C–X. However, it was not observed, with an estimated sensitivity (including the effects of laser intensity) about $^1/_3$ that obtained for the G–X scan.

Term Values from Fluorescence Scans

With the laser wavelength set on a particular excitation transition, the monochromator can be scanned to provide fluorescence

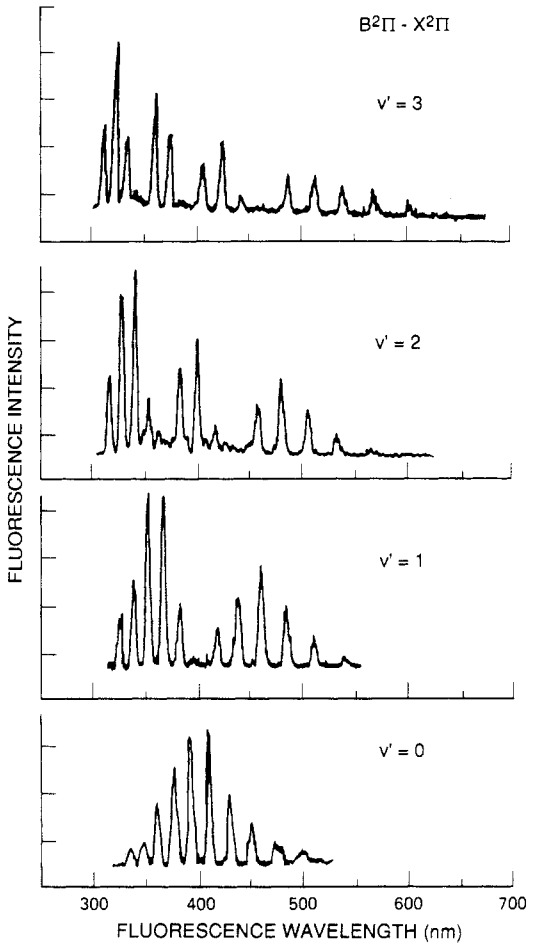

Figure 7. Scans of fluorescence from four vibrational levels in the $B^2\Pi$ state. For the spectrum in each panel, the laser is tuned to excite that v' and the monochromator is scanned. The band intensities have not been corrected for monochromator/detector response. The pattern seen, which looks like the upper-state vibrational probability distributions, arises from the positioning of the B and X potential curves, as explained in the text.

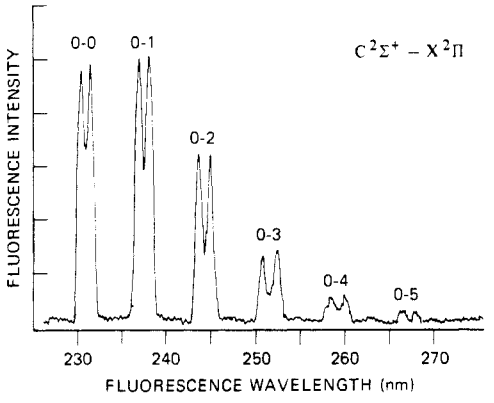

Figure 8. Fluorescence scans for the $v' = 0$ level of the $C^2\Sigma^+$ state, uncorrected for response.

spectra. In the absence of collisions, these provide two types of information. The first are vibrational term values, often of very high v'' in the ground state. The second are vibrational band transition probabilities, related to Franck–Condon factors and an electronic transition moment.[15] Again, the lack of interfering transitions makes LIF, when applicable, a choice method[11] for determination of such quantities in complex and extensive band systems such as $B^2\Pi$–$X^2\Pi$ studied here.

Figures 7, 8, and 9 show fluorescence spectra upon excitation of specific vibrational level(s) in the $B^2\Pi$, $C^2\Sigma^+$, and $A^2\Delta$ states,

(15) Crosley, D. R.; Lengel, R. K. *J. Quant. Spectros. Radiat. Transfer* **1975**, *15*, 579.

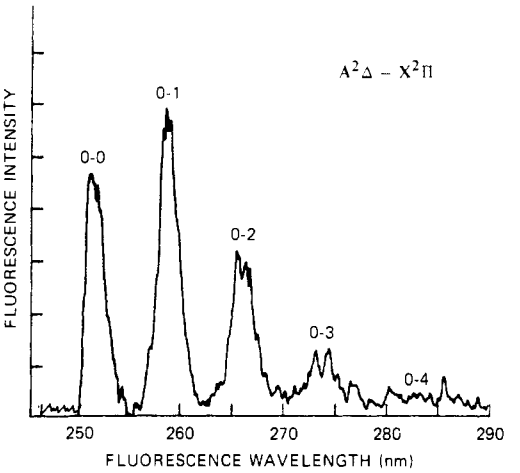

Figure 9. Fluorescence scans for the $v' = 0$ level of the $A^2\Delta$ state, uncorrected for response.

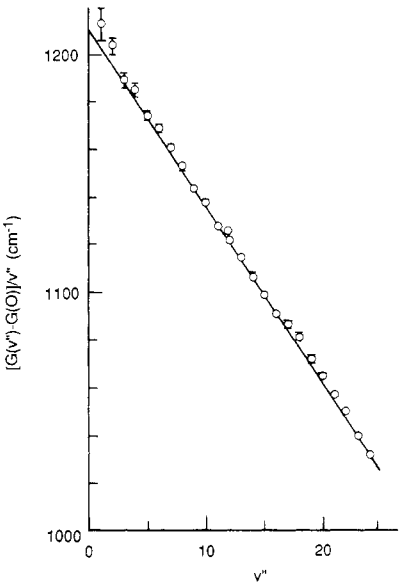

Figure 10. A plot of the quantity $[G(v'') - G(v''=0)]/v''$ vs v'' for the $X^2\Pi$ state, from fluorescence scans for all three electronic systems studied. The plot has an intercept of $\omega_e - \omega_e x_e$ and a slope of $-\omega_e x_e$. Error bars shown are $1 - \sigma$ values from the averaging over different determinations.

TABLE I: Vibrational Constants for NS $X^2\Pi$

	quadratic fit	cubic fit
ω_e	1219.90 ± 1.1	1218.50 ± 2.5
$\omega_e x_e$	7.45 ± 0.06	7.24 ± 0.34
$\omega_e y_e$		−0.007 ± 0.011

respectively. From the positions of the bands shown, the ground-state vibrational term values can be extracted. These extend to much higher vibrational levels ($v'' = 26$) than in previous measurements, which rarely went above $v'' = 2$ and never higher than $v'' = 6$.

The vibrational band frequencies were taken from the wavelengths at the peak for bands of low resolution where the spin–orbit splitting was unresolved (see, e.g., Figure 7 and low v'' in Figure 9), or the minimum point between resolved peaks as in Figure 8. To obtain the vibrational constants in the expression

$$G(v) = \omega_e(v + \tfrac{1}{2}) - \omega_e x_e(v + \tfrac{1}{2})^2 + \omega_e y_e(v + \tfrac{1}{2})^3 \quad (1)$$

the data were cast into the form $[G(v') - G(0)]/v''$ for fitting vs v''. The plot is shown in Figure 10. It is quite linear with little curvature, suggesting that the cubic term $\omega_e y_e$ is small. The points have been least-squares fit to both quadratic and cubic equations, with the results given in Table I. Note that, in the cubic fit, the

TABLE II: Franck-Condon Factors and Uncertainties for $v' = 0$–2 of the B–X System[a]

	$v' = 0$					$v' = 1$					$v' = 2$				
	$p_{v'v''}$	$q_{v'v''}$				$p_{v'v''}$	$q_{v'v''}$				$p_{v'v''}$	$q_{v'v''}$			
v''	expt	RKR	Morse	δp	Δp	expt	RKR	Morse	δp	Δp	expt	RKR	Morse	δp	Δp
0	13	3	3	3	3	31	13	16	11	11	36	33	42	5	6
1	29	18	21	8	9	73	62	72	5	8	115	108	120	5	11
2	61	59	67	7	10	146	129	137	7	14	140	120	115	9	10
3	147	124	134	9	20	151	139	135	10	16	40	36	24	5	6
4	195	186	192	9	25	74	68	56	11	13	9	4	11	2	2
5	193	206	205	22	32	8	3	1	1	1	78	72	82	3	7
6	155	177	170	10	21	41	28	38	5	6	104	93	86	6	11
7	108	120	112	21	25	114	109	119	9	13	29	27	17	4	5
8	52	65	59	5	8	143	159	160	9	15	7	4	10	1	1
9	33	29	25	16	16	116	142	135	4	12	77	72	87	5	8
10	14	10	9	9	9	68	89	81	4	7	138	141	146	11	16
11		3	2			28	42	36	3	4	124	140	133	11	15
12						6	15	12	6	6	78	90	80	10	12
13							4	3			25	41	34	6	6
14												14	10		

[a] Entries are actual values multiplied by 1000.

TABLE III: Franck-Condon Factors and Uncertanties for $v' = 3$–5 of the B–X System[a]

	$v' = 3$				$v' = 4$				$v' = 5$			
	$p_{v'v''}$	$q_{v'v''}$			$p_{v'v''}$	$q_{v'v''}$			$p_{v'v''}$	$q_{v'v''}$		
v''	expt	RKR	δp	Δp	expt	RKR	δp	Δp	expt	RKR	δp	Δp
0	64	65	2	8	95	92	3	7	106	114	8	17
1	125	123	6	16	107	98	3	7	54	53	4	9
2	57	51	4	8	4	3	1	1	16	11	2	3
3	18	3	4	5	61	48	3	5	82	70	5	12
4	86	69	3	11	68	60	3	5	9	7	1	2
5	62	61	3	8	1	<1	1	1	50	36	3	8
6	11	1	4	4	66	50	2	5	61	51	2	9
7	62	44	2	8	63	57	3	5	3	<1	1	1
8	84	86	4	11	1	1	1	1	68	51	2	10
9	25	31	3	4	51	44	2	3	46	44	4	8
10	8	3	5	5	77	79	6	8	3	<1	1	1
11	75	71	4	10	16	20	2	2	66	58	5	10
12	126	140	19	24	15	10	2	2	62	66	2	9
13	94	132	11	16	93	91	5	8	4	5	2	2
14	49	78	20	21	127	144	6	10	41	33	8	10
15	31	32	4	6	91	116	7	9	124	121	12	21
16	<24	9	24	24	42	59	4	5	111	141	25	29
17		2			21	20	10	10	69	90	26	28
18						5			26	37	26	26

[a] Entries are actual values multiplied by 1000.

$\omega_e y_e$ value overlaps zero within its uncertainty, and standard deviations are higher. Clearly, the quadratic expression is preferable; that is, there is no discernible cubic anharmonicity even at these very high v'', up to two-thirds of the dissociation limit.

Transition Probabilities from Fluorescence Scans

The intensity of fluorescence in a given vibrational band (v', v'') at wavelength $\lambda_{v''}$ is proportional to the Einstein coefficient $A_{v',v''}$ for spontaneous emission (s^{-1} units) in that band; the vibrational transition probability $p_{v',v''}$ is then

$$p_{v',v''} \propto A_{v',v''}\lambda_{v',v''}^3 \tag{2}$$

We may write $p_{v',v''}$ as an integral of the electronic transition moment $R_e(r)$ times the upper and lower state vibrational wave functions ϕ_v over the internuclear distance r

$$p_{v',v''} = |\int \phi(r)_{v'} R_e(r) \phi_{v''}(r) \, dr|^2 \tag{3}$$

where $R_e(r)$ is the integral of the transition dipole moment fraction times the electronic wave functions involved, taken over the electronic coordinates. Generally, the form of $R_e(r)$ is not known, although modern ab initio calculations can usually provide realistic values. If R_e is constant as a function of r with the value $\bar{R}_e$, then eq 3 assumes the simple form

$$p_{v',v''} = \bar{R}_e^2 q_{v',v''} \tag{4}$$

where $q_{v',v''}$ is the Franck–Condon factor or the square of the vibrational overlap integral

$$q_{v',v''} = |\int \phi_{v'}\phi_{v''} \, dr|^2 \tag{5}$$

If the known or estimated functional form of $R_e(r)$ is simple enough, then the r-centroid approximation can be used to calculate $p_{v',v''}$

$$p_{v',v''} = [R_e(\bar{r}_{v',v''})]^2 q_{v',v''} \tag{6}$$

Here the r-centroid

$$\bar{r}_{v',v''} = \int \phi_{v'} r \phi_{v''} \, dr / \int \phi_{v'}\phi_{v''} \, dr \tag{7}$$

When $R_e(r)$ is linear, $R_e(r) = c(1 - \rho r)$.

A. Experimental Results. With the laser wavelength fixed so as to excite the v' level in an excited state, the monochromator was scanned to record the fluorescence spectrum of all (v',v'') bands having nonzero intensity. (The fluorescence spectrum for $B^2\Pi$, $v' = 12$, was too weak to provide reliable results, and is not included here.) Such spectra are shown in Figures 7, 8, and 9 for the states $B^2\Pi$, $C^2\Sigma^+$, and $A^2\Delta$, respectively. The intensities of the bands (together with the monochromator/detector response calibration) were used to obtain relative $A_{v',v''}$, which were then converted to $p_{v',v''}$ by using eq 2. The wavelength $\lambda_{v',v''}$ was the same used to determine the vibrational constants discussed in the preceding section. The $p_{v',v''}$ are listed as the first entry in each

TABLE IV: Franck-Condon Factors and Uncertainties for $v' = 6$–8 of the B–X System[a]

	$v' = 6$				$v' = 7$				$v' = 8$			
v''	$p_{v'v''}$ expt	$q_{v'v''}$ RKR	δp	Δp	$p_{v'v''}$ expt	$q_{v'v''}$ RKR	δp	Δp	$p_{v'v''}$ expt	$q_{v'v''}$ RKR	δp	Δp
0	131	124	6	17	120	121	3	9	137	109	5	16
1	17	15	2	3	2	<1	1	1	24	8	1	3
2	55	46	4	8	74	65	2	6	74	56	7	11
3	47	39	3	6	6	5	3	3	11	5	1	2
4	15	10	2	3	54	49	2	4	66	50	2	8
5	73	57	2	9	22	20	1	2	4	<1	2	2
6	2	2	1	1	29	21	1	2	72	48	2	9
7	57	42	3	7	49	42	2	4	5	3	1	1
8	43	35	2	5	3	1	1	2	57	38	3	7
9	8	4	1	1	61	51	2	5	24	20	2	3
10	67	59	2	8	13	13	2	2	26	16	1	3
11	21	23	2	3	28	22	3	4	52	46	6	9
12	16	11	2	3	56	56	2	5	2	<1	2	2
13	70	73	6	10	2	3	2	2	58	48	8	10
14	31	39	2	4	43	40	2	4	24	31	4	5
15	3	2	3	3	65	70	5	7	10	6	2	2
16	83	76	13	16	8	8	3	3	64	70	12	14
17	127	144	16	22	51	31	3	5	25	37	4	5
18	115	121	34	37	125	126	12	15	8	4	4	4
19	17		17	17	125		19	21	91		10	15
20					64		6	8	96		18	21
21									51		15	16
22									18		9	9

[a] Entries are actual values multiplied by 1000.

TABLE V: Franck-Condon Factors and Uncertainties for $v' = 9$–11 of the B–X System[a]

	$v' = 9$				$v' = 10$				$v' 11$			
v''	$p_{v'v''}$ expt	$q_{v'v''}$ RKR	δp	Δp	$p_{v'v''}$ expt	$q_{v'v''}$ RKR	δp	Δp	$p_{v'v''}$ expt	$q_{v'v''}$ RKR	δp	Δp
0	99	91	3	12	80	72	3	11	40	54	2	5
1	39	29	2	5	69	50	6	11	64	65	3	8
2	33	30	5	6	15	8	3	4	1	<1	1	1
3	41	29	5	7	68	48	8	12	54	46	2	7
4	30	23	2	4	6	1	2	2	10	6	3	3
5	33	23	1	4	67	43	8	12	37	33	2	5
6	32	26	3	5	3	1	1	1	14	10	3	3
7	25	14	2	3	65	40	3	9	34	28	2	4
8	46	35	2	6	6	3	2	2	16	10	1	2
9	8	44	5	5	59	36	2	8	40	29	5	7
10	63	44	11	13	15	9	1	2	13	7	1	2
11	<1	1	1	1	46	27	3	7	46	35	4	7
12	56	41	7	9	33	24	1	4	6	2	1	1
13	15	19	2	3	18	11	3	4	49	41	7	9
14	19	15	2	3	58	44	2	8	3	1	1	1
15	45	54	2	5	2	<1	1	1	52	40	3	7
16	3	2	3	3	62	48	5	9	15	13	4	4
17	58	43	5	8	18	23	3	4	29	23	2	4
18	60	63	4	8	14	14	4	4	52	46	2	6
19	4		4	4	56		8	11	9		3	3
20	68		5	9	9		4	4	74		3	9
21	110		12	17	34		6	7	20		4	4
22	69		7	12	86		13	17	19		5	5
23	25		8	8	72		16	18	105		11	17
24	20		10	10	39		19	20	113		7	15
25									57		16	17
26									30		20	20

[a] Entries are actual values multiplied by 1000.

of the Tables II–V. Note that the table entries are all 1000 times the stated quantity, e.g., $p_{0,0} = 0.013$. The values in the table are normalized so that the sums over v'' equal unity; they thus form vibrational transition probabilities or branching ratios which can be used with radiative lifetimes to calculate absolute absorption and emission coefficients. For conversion of the $p_{v',v''}$ back to Einstein coefficients $A_{v',v''}$ via eq 2, the wavelengths may be determined by using eq 1, $\nu_{0,0} = 30019.35$ cm^{-1}, ω_e' and $\omega_e x_e'$, and the constants of Table I. (Note that for precision better than 2%, when each spin–orbit component is separately considered, one should use the actual wavelength for each subband.)

There are two types of errors associated with each entry. The first, denoted $\delta p_{v',v''}$, is the relative error among the set of $p_{v',v''}$ for a given v'. This is caused by experimental uncertainty in both the fluorescence intensity measurement and the monochromator/detector calibration. Several runs were made for each v' (at least four, and as many as seven). The average values and statistical uncertainties were computed. To form $\delta p_{v',v''}$, these uncertainties are then added in quadrature with that from the calibration, which is typically 2% but somewhat larger near both ends of the wavelength range covered. The second type of error, listed as $\Delta p_{v',v''}$, is that associated with the absolute value of $p_{v',v''}$. It includes the additional error resulting from the normalization and is that error pertinent to a calculation of absolute absorption or emission coefficients. $\Delta p_{v',v''}$ is obtained by adding in quadruture the quantity $\delta p_{v',v''}$ plus the error in which the normalizing sum

TABLE VI: Franck–Condon Factors for $v' = 0$ of the C–X System[a]

v''	$p_{v'v''}$ expt	$q_{v'v''}$ Morse	$\bar{r}_{v'v''}$, Å	$p_{v'v''}$ calcd	$\delta p_{v'v''}$	$\Delta p_{v'v''}$
0	549	634	1.472	578	16	25
1	300	281	1.423	302	8	13
2	93	70	1.373	92	3	4
3	43	13	1.322	21	2	3
4	12	2	1.275	6	2	2
5	4	0.3	1.230	1	2	2

[a] Entries are actual values multiplied by 1000.

for each v' differs from unity due to errors in the individual $p_{v',v''}$, i.e., $\sum \delta p_{v',v''}$.

In the following sections, we discuss in turn the interpretation of the measured $p_{v',v''}$ for each of the B–X, C–X, and A–X transitions, followed by a brief pictorial description of the B–X Franck–Condon pattern.

B. B–X Transition Probabilities. No prior information exists concerning the form of $R_e(r)$ for the B–X system of NS. We can examine the question empirically by comparing the measured $p_{v',v''}$ with reliably calculated values of $q_{v',v''}$. Any systematic deviation with increasing $\bar{r}_{v',v''}$ will signal a variation of R_e with internuclear distance.

In the second columns for each v', in Tables II–V, are listed $q_{v',v''}$ calculated from RKR potentials for the B and the X states[16,17] by using the standard set of B–X constants from ref 6, 9, and 10. Those investigations did not extend to the high values of v'' needed here and calculated in ref 16. However, recall that we found that no cubic $\omega_e y_e$ term was needed as high as $v'' = 26$ in the expression for $G_{v''}$, eq 1, so that the ω_e and $\omega_e x_e$ used in ref 16 should form a valid representation of the potential.

An examination of the experimental $p_{v',v''}$ and the $q_{v',v''}$ calculated from RKR potentials shows an astoundingly good agreement over the entire range of vibrational levels covered here, $v' = 0$–11 and $v'' = 0$–26. We can use the comparison between the $p_{v'v''}$ and the $q_{v'v''}$ to establish a limit on the variation of R_e with internuclear distance. Assuming $R_e(r) = c(1 - \rho r)$, a value of $\rho \geq \pm 0.02$ produces calculated $p_{v'v''}$ from the RKR $q_{v'v''}$ which have significantly larger average deviation than those obtained by using a constant R_e. According to the RKR calculations, the r centroid varies from a minimum of less than 1.46 Å for the (11,0) band to greater than 2.40 (Å ($\bar{r}_{v',v''}$ for (0,18)); therefore, a large range of internuclear distance is sampled by this set of vibrational bands. Also, this good agreement between the $p_{v',v''}$ and the $q_{v',v''}$ forms a very stringent test of the RKR potentials used. This is because the high degree of cancellation in the integrals of eq 5 would be changed considerably with a slight shift in $G(v'')$. Consequently, the B–X transition in NS can be considered well characterized and understood as regards both spectral line positions and band intensities.

The $q_{v',v''}$ may also be summed over v' for a given v''. This sum differs from unity by an amount which represents the overlap with $v' = 12$ and the continuum $B^2\Pi$ levels above the predissociation limit. As in the case[12] of the B–X system of S_2, the sum is nearly unity (0.95) for $v'' = 0$ and decreases for higher v''.

The Franck–Condon factors $q_{v',v''}$ calculated by using Morse wave functions with the same constants as in the RKR curves are also included in Table II, in the third columns for each of the levels $v' = 0$, 1, and 2. The correspondence of the positions of all minima and maxima and the quantitative agreement for strong bands is excellent. Although the RKR calculations should be more accurate, the Morse wave function calculations are included here to show that they are sufficiently reliable for low vibrational levels. They will be used for the calculations on the C–X and A–X systems, as RKR potentials are not available for the C and A states.

TABLE VII: Franck–Condon Factors for $v' = 0$ and 1 of the A–X System[a]

v''	$p_{v'v''}$ expt	$q_{v'v''}$, Morse $r_e = 1.59$ Å	$r_e = 1.58$ Å	$\delta_{pv'v''}$	$\Delta p_{v'v''}$
		$v' = 0$			
0	291	231	308	52	64
1	409	360	377	34	62
2	201	256	216	12	28
3	77	111	76	18	20
4	23	33	19	10	10
5		7	3		
		$v' = 1$			
0	238	307	336	30	38
1	46	51	11	3	5
2	247	61	135	22	32
3	284	234	263	11	29
4	140	210	173	18	22
5	36	99	64	6	7
6	9	1		5	5

[a] Entries are actual values multiplied by 1000.

C. C–X Transition Probabilities. Table VI lists the experimental results and also $q_{v',v''}$ calculated with Morse wave functions. Only the $v' = 0$, 1, and 2 levels of the C state have been observed.[7,17] The spacing is not regular, so that reliable values of ω_e' and $\omega_e x_e'$ do not exist. We chose $\omega_e' = 1414$ cm^{-1} and $\omega_e x_e' = 5.25$ cm^{-1}; test calculations with other combinations showed that the conclusions concerning $R_e(r)$ are not sensitive to the precise values. Here, the $p_{v',v''}$ and $q_{v',v''}$, columns 2 and 3, do not match as they did in the B–X system. There is a smooth decrease in $q_{v',v''}/p_{v',v''}$ with increasing v''. This is in the opposite direction of the smoothly decreasing $\bar{r}_{v',v''}$, column 4, indicating a decrease in $R_e(r)$ with increasing r.

In the case of the C–X system of NS, there exists an ab initio calculation of the electronic transition moment[19] as a function of internuclear distance. Over the range corresponding to the r centroids given in Table VI, $R_e(r)$ decreases with increasing r, at first more rapidly, then more gradually beginning at about 1.3 Å.

Values of $R_e(\bar{r}_{v',v''})$ were taken graphically from Figure 5 of ref 19 (including an extrapolation to $\bar{r}_{0,6}$) and used in eq 6 to calculate $p_{v',v''}$. The results are listed in column 5 of Table VI. The values for the three strongest bands are in excellent agreement with observation; the ab initio moment is nearly linear and eq 6 exact in the region of internuclear distance which corresponds to those $\bar{r}_{v',v''}$. For the weaker bands, $v'' = 3$, 4, and 5, the calculation predicts values lower than measured, but these are bands that have an intensity only 1–8% of that of the strong bands and here the variation of the ab initio moment is no longer linear. As with the B–X system of NS, it appears that the C–X, $v' = 0$ sequence transition probabilities are well understood.

Franck–Condon factors were also calculated for the $G^2\Sigma^- - X^2\Pi$ transition, using the Morse wave functions. This was for the purpose of assessing the relative magnitudes of the LIF signals from the G compared to the C state (Figure 5). The results showed large $q_{v',v''}$ (0.2–0.3) for the bands observed in the experiment, indicating that a poor choice of fluorescent band was not the reason for the much lower signal levels relative to C–X seen here, compared to those in emission studies.

D. A–X Transition Probabilities. Vibrational transition probabilities were measured for $v' = 0$ and 1 (see Table VII). Here, as for C–X bands, the measured $p_{v',v''}$ do not correspond to the $q_{v',v''}$ calculated with the Morse wave functions by using the nominal spectroscopic constants[6] including the tablulated[20] value for internuclear equilibrium distance in $v' = 0$, $r_0 = 1.59$

(16) Raghuveer, K.; Narasimham, N. A. *J. Astrophys. Astron.* **1982**, *3*, 13.

(17) There are two misprints in Table 3 of ref 16. The entry for $q_{0,3}$ should read 0.124, as determined by summing the $q_{0,v''}$ to unity. $q_{9,10}$ and $q_{9,9}$ are both listed as 0.0421, but the calculations do not extend to high enough values of v'' to take a sum; here, the Morse wave functions are not reliable enough to furnish a value.

(18) Chiu, C.-L.; Silvers, S. J. *J. Chem. Phys.* **1975**, *63*, 1095.

(19) Lie, G. C.; Peyerimhoff, S. D.; Buenker, R. J. *J. Chem. Phys.* **1985**, *82*, 2672.

(20) Huber, K. P.; Herzberg, G. *Constants of Diatomic Molecules*; Van Nostrand: New York, 1979.

TABLE VIII: Fluorescence Lifetime (ns) of $A^2\Delta$ (N_2 = 1 Torr, SF_6 = 40 mTorr)

	$A^2\Delta_{3/2}$	$A^2\Delta_{5/2}$
$v' = 0$	100	140
$v' = 1$	290	290

Å (columns 2 and 3). In this case, however, there is no smooth variation of $p_{v',v''}/q_{v',v''}$ with vibrational level, which would have indicated an $R_e(r)$ varying in a simple fashion. Particularly striking is the disagreement between the observed ratio $p_{1,2}/p_{1,1} > 5$ compared with the calculated ratio of approximately unity.

The effects of using a smaller r_e to construct the Morse wave functions were then explored. The value of r_e is smaller than r_0, due to anharmonicity in the potential and the fact that the rotational constant B is actually an average over $1/r^2$. The result for r_e = 1.58 Å is given in column 4 of Table VII. This shows excellent agreement for the $v' = 0$ sequence, with the intensities of all bands predicted to within experimental error. This calculation yields a better value for the troublesome ratio $p_{1,2}/p_{1,1}$, although none of the $v' = 1$ bands is predicted well. Varying the anharmonicity between 1 and 10 cm^{-1}, as expressed in the Morse wave function, did not bring about better agreement for $v' = 1$ without lessening it considerably for $v' = 0$. This transition appears not as well characterized as those from the B and the C states.

E. The B–X Intensities. The B–X fluorescence spectra plotted in Figure 7 display reflection structure.[21,22] That is, the radial probability distribution in the excited state is displayed in the vibrational band intensity variation of the fluorescence to the lower state.[23-25] This occurs when the difference potential $V(r) = V'(r) - V''(r)$ is monotonic in the region sampled by the excited state wave function. The number of peaks and nodes in the excited-state probability distribution are conserved. This reflection structure provides a convenient method to determine if there are more vibrational bands from a given v'. One need only ensure that $v' + 1$ nodes have been observed in the band structure and an upper bound of the vibrational band strength for any band to the red of the last band tabulated in Tables II–V is apparent.

Lifetime Measurements

The time decay of the fluorescence was observed on an oscilloscope upon excitation of each individual level, and quantitative measurements were made with the transient digitizer for a few levels. In the latter case, extrapolation to zero pressure in the discharge flow apparatus was necessary to obtain a radiative decay rate. The measured results are collected in Table VIII.

The $C^2\Sigma^+$, $v' = 0$ lifetime was <15 ns, too short to be measured with our apparatus. This is consistent with the value of 6.5 ns determined by using Hanle effect measurements with resonance lamp and atomic line excitation.[26] This value is considerably faster than the radiative lifetime of 30 ns calculated[19] from ab initio wave functions. It therefore seems likely that the short lifetime is due to predissociation.[18]

The $B^2\Pi$ lifetimes, up to $v' = 11$, were all observed to be in the neighborhood of 1 μs, a typical value for a valence excited state of this nature in a diatomic molecule. This is in good agreement with the radiative rate results determined accurately for $v' = 6$–9 in ref 2. The observed decay rates in the presence of N_2 for $v' = 3$, 10, and 11 are also in agreement with the results of ref 2 for the decay of those levels due to both radiative and quenching contributions.

The situation for $v' = 12$, the highest bound level, is different in that here collisions appear to be much more effective in removing the NS from the radiating B state. This is no doubt due to collision-induced predissociation. Matsumi et al.[2] report removal cross sections some 5-fold higher for $v' = 12$, and those for two different rotational levels in $\Omega = {}^3/_2$ are 50% larger than for $\Omega = {}^1/_2$. We also find a large variation in lifetimes with J and Ω. In the low-J region excited in the R_2 head (see Figure 4), the lifetime in the presence of 100 mTorr of N_2 and 30 mTorr of SF_6 is ~200 ns; for the $P_2(7.5)$ line it was >100 ns; and for $P_2(14.5)$ it was ≪100 ns. The lifetime of the $\Omega = {}^1/_2$ level was longer, even though it was this level whose excitation scan exhibited more perturbations as evidence by anomalous Λ-doublet splitting. We suggest that the collisions are not directly mixing the initially pumped levels with predissociating states but are causing rotational energy transfer to levels above the dissociation limit. Rotational energy transfer is facile in the lower vibrational levels of the B state.[1] A thermal distribution of rotational levels in the $\Delta = {}^3/_2$ component of the B state has a larger fractional population in rotational levels above the dissociation limit than the $\Omega = {}^1/_2$ component. This alone can account for the difference in fluorescence lifetimes after different levels are excited.

Lifetimes in the $A^2\Delta$ state also show an irregular dependence upon vibrational level and spin–orbit component; this can also be attributed to predissociation, both spontaneous and collision-induced. These measurements were made in the presence of 1 Torr of N_2 and 40 mTorr of SF_6. Table VIII contains the results. In this case, there appears to be a loss mechanism of $v' = 0$ which is not as strong for $v' = 1$; on the other hand, the rotational analysis of the A–X transition in ref 6 indicated it is $v' = 1$ which is more perturbed. Also, the present results suggest that in $v' = 0$, the $^2\Delta_{3/2}$ component is more easily collisionally predissociated than $^2\Delta_{5/2}$, an effect attributable to mixing with a $^2\Pi$ or a $^4\Sigma$ state.

Conclusion

We have measured the vibrational band transition probabilites for a total of 251 bands of the B–X, C–X, and A–X systems of NS. These measurements show that the RKR potential for the $B^2\Pi$ state is well characterized and the electronic transition moment for the B–X system does not vary with internuclear distance. However, for the C–X system, $R_e(r)$ decreases with increasing r. These transition moments make quantitative detection of NS[1,4] possible. The excitation spectra of $v' = 0$–12 of B–X exhibit numerous perturbations due to the $B'^2\Sigma^+$, $a^4\Pi$, and $b^4\Sigma^-$ states. The collisional predissociation of $v' = 12$ of $B^2\Pi$ and $v' = 0$ of $A^2\Delta$ appears to have spin–orbit state specificity. The existence of many nearby excited electronic states, which have different electronic structure and are each accessible to laser excitation, makes this radical a choice candidate for further collision studies.

Acknowledgment. We acknowledge Fred Kaufman, whom each of us knew as a friend and respected as a scientist and teacher. J.B.J., who worked as a postdoctoral associate with Professor Kaufman from 1980 to 1983, especially notes his appreciation for the guidance and discussions which changed the way he thinks about science. This research was supported by the NSF Thermal and Systems Engineering Program through grant CPE-8319610. The computer used was furnished through NSF on grant PHY-8114611.

Registry No. NS, 12033-56-6.

(21) Tellinghuisen, J.; Pichler, G.; Snow, W. L.; Hillard, M. E.; Exton, R. J. *Chem. Phys.* **1980**, *50*, 313.
(22) Tellinghuisen, J. *J. Mol. Spectrosc.* **1984**, *103*, 455.
(23) Hunt, P. M.; Child, M. S. *Chem. Phys. Lett.* **1978**, *58*, 202.
(24) Mulliken, R. S. *J. Chem. Phys.* **1971**, *55*, 309.
(25) Noda, C.; Zare, R. N. *J. Mol. Spectrosc.* **1982**, *95*, 254.
(26) Silvers, S. J.; Chiu, C.-L. *J. Chem. Phys.* **1974**, *61*, 1475.